Geophys. J. Int. (1998) **135**, 388–406

Computation of seismograms and atmospheric oscillations by normal-mode summation for a spherical earth model with realistic atmosphere

Philippe Lognonné,[1,2] Eric Clévédé[2] and Hiroo Kanamori[3]

[1] *Département des Etudes Spatiales, Institut de Physique du Globe de Paris,* 4 *Avenue de Neptune,* 94107 *Saint Maur des Fosses Cedex, France*
[2] *Département de Sismologie,* UMR7580, *Institut de Physique du Globe de Paris,* 4, *Place Jussieu,* 75252 *Paris Cedex, France.*
E-mail: lognonne@ipgp.jussieu.fr
[3] *Seismological Laboratory, California Institute of Technology,* 251 *S. Mud, Pasadena,* CA91125, *USA*

Accepted 1998 June 3. Received 1998 April 10; in original form 1997 August 1

SUMMARY

We describe a theory to compute seismograms and atmospheric disturbances such as ionospheric oscillations or pressure variations in a realistic spherical earth model with atmosphere. This theory is valid for a source located either in the solid earth or in the atmosphere. Solid earth and atmospheric normal modes are computed for a radiation boundary condition that models the dissipation of acoustic signals in the high atmosphere of the Earth. We show that the coupling between ground and atmosphere occurs at a set of frequencies related to fundamentals and harmonics of atmospheric modes. Spheroidal modes near these frequencies have up to 0.04 per cent of their energy in the atmosphere, and thus may be strongly excited by atmospheric sources. This theory can be used for more accurate modelling of the seismic data from meteoritic events or volcanic eruptions as well as for the analysis of barograms or ionograms recorded after large earthquakes.

Key words: acoustic impedance, atmosphere, explosion seismology, ionosphere, normal modes, seismograms.

1 INTRODUCTION

The atmosphere of the Earth is generally considered decoupled from the solid Earth. The Earth's solid surface is then considered either as a free surface (by seismologists) or as a rigid surface (by atmosphericists). However, it has been recognized that solid Earth sources such as earthquakes can excite the atmosphere, and atmospheric sources such as nuclear, meteoritic or volcanic explosions can excite the solid Earth.

Atmospheric disturbances were observed by Yuen *et al.* (1969) and Weaver *et al.* (1970) following large earthquakes. These signals were measured by Doppler records, sensitive to the ionospheric disturbances, and are related to acoustic head waves excited by the surface Rayleigh waves. Such waves probably also produce variations in the total electronic content (TEC) observed by GPS satellites after earthquakes (Calais & Minster 1995). Indeed, due to the exponential decrease of the density with height, the small displacement of the surface waves at ground level is strongly amplified, by a factor of more than 10 000, when the head wave propagates vertically. Displacements of the order of 100 m associated with velocities of 20 m s^{-1} are then found at epicentral distances of about 90° for earthquakes of magnitude $M_s = 7.9$ (Parrot *et al.* 1993). For a review of atmospheric and ionospheric disturbances, see Pokhotelov *et al.* (1998).

In an opposite manner, atmospheric sources produce seismic signals. Seismograms were recorded following the Siberian Tunguska explosion (Ben-Menahem 1975) and other meteorite impacts (e.g. Cevolani 1994). Signals were also reported following the 1991 volcanic eruption of Pinatubo (Kanamori & Mori 1992; Widmer & Zürn 1992; Zürn & Widmer, 1996; Kanamori *et al.* 1984) and the 1982 El Chichon eruption (Zürn & Widmer 1996). These data, as well as the recent discovery of the apparent excitation of normal modes by atmospheric turbulence (Suda *et al.* 1998; Tanimoto 1998; Tanimoto *et al.* 1998), have renewed the attention of seismologists to the problem of coupling between the solid Earth and the atmosphere. The 1991 eruption of Mount Pinatubo excited harmonic fundamental-mode Rayleigh waves with periods of about 230 and 270 s that were believed to be caused by acoustic coupling of the solid Earth and the atmosphere. A very detailed study of this data set is given by Watada (1995). Similar problems

were investigated for the Shoemaker–Levy 9 comet impact on Jupiter. The excitation by this impact of seismic waves (Kanamori 1993; Lognonné *et al.* 1994) and gravity waves (Ingersoll *et al.* 1994) has been investigated. Although seismic waves were not observed (Mosser *et al.* 1996), some ring-like patterns observed immediately after the impact have been interpreted as gravity waves (Ingersoll & Kanamori 1995; Hammel *et al.* 1995).

The objective of this paper is to investigate the excitation and propagation problems in a coupled system of the solid Earth and the atmosphere by considering a unique model from the centre of the Earth to the top of the atmosphere. A seismic or atmospheric source can then be considered at any location using the seismic source tensor (Backus & Mulcahy 1976a,b) for the solid Earth, and a generalization of it for the atmosphere. The latter was used by Lognonné *et al.* (1994) to estimate the seismic source produced by the impact of the comet Shoemaker–Levy in the Jovian atmosphere. In the same way, barograms, temperature fluctuations or displacement of the ionized layers, can be computed by the summation of normal modes for the solid Earth–atmosphere system.

In particular, we first show that the new boundary condition imposed by the infinite, exponentially rarefying atmosphere of the Earth and described by Watada (1995), requires a different formulation for both the eigenproblem and the normal-mode summation for the computation of seismograms. We then describe an efficient numerical method for the computation of these normal modes. The formalism of the normal-mode summation for the computation of seismograms or barograms is then described. Finally, an example of the synthetic signal of the seismic signal induced by an explosive source in the atmosphere is shown.

2 THEORY

For the whole planet, the linearized elastodynamic equation in the non-rotating case can be written in a general Eulerian form:

$$\partial_{t^2}\mathbf{u} = -\mathbf{A}(\mathbf{u}) = \frac{1}{\rho}\left[\boldsymbol{\nabla}.(\mathbf{T}_{\text{elastic}} - \mathbf{u}.\boldsymbol{\nabla}\mathbf{T}_0) - \text{div}(\rho\mathbf{u})\mathbf{g} - \rho\boldsymbol{\nabla}\Phi_{E_1}\right], \tag{1}$$

where $\mathbf{u}$ is the displacement, ρ is the unperturbed density, $\mathbf{T}_{\text{elastic}}$ is the strain-generated departure from equilibrium, $\mathbf{g}$ is the gravity and Φ_{E_1} is the mass redistribution potential. The equilibrium stress $\mathbf{T}_0$ is the solution of the following:

$$\boldsymbol{\nabla}.\mathbf{T}_0 + \rho\mathbf{g} = 0. \tag{2}$$

Relation (1) defines the gravito-elastic operator $\mathbf{A}(\mathbf{u})$. This relation applies to either the liquid, the solid or the gaseous part of the atmosphere. The only difference is found in the constitutive relation of the elastic stress $\mathbf{T}_{\text{elastic}}$. In the solid parts, a symmetric stiffness tensor is generally used, which gives

$$\mathbf{T}^{ij}_{\text{elastic}}(\mathbf{r}, t) = C^{ijkl} D_k u_l(\mathbf{r}, t). \tag{3}$$

In the isotropic solid parts, we have $C^{ijkl} = [\kappa - (2/3)\mu]g^{ij}g^{kl} + \mu(g^{ik}g^{jl} + g^{il}g^{jk})$, where κ is the bulk modulus and μ is the shear modulus. g^{ij} is the metric tensor, equivalent to the Kroenecker symbol in Cartesian coordinates (g^{ij} is non-zero and equal to 1 for $i=j$ only). In the fluid parts (either liquid or gaseous) we have $C^{ijkl} = \kappa g^{ij}g^{kl}$. In parallel to these equations, we also have all the continuity relations, related to the continuity of stress and displacement on all solid/solid discontinuities, and of stress and vertical displacement on all solid/fluid or fluid/fluid discontinuities. For solid/solid interfaces, they are defined by the continuity of displacements and by the continuity of the stress vector associated with all horizontal interfaces, which can be written as

$$\mathscr{M}_0(\mathbf{u}) = \mathbf{T}_{\text{elastic}}(\mathbf{r}, t).\mathbf{n}, \tag{4}$$

where $\mathbf{T}_{\text{elastic}}$ is the stress associated with the displacement $\mathbf{u}$, as defined in (3), and $\mathbf{n}$ is the radial normal vector. In the liquid/solid interface, we have only the continuity of the vertical displacement, and only the radial component of the stress is non-zero and equal to pressure. The boundary operator will therefore be written in the following in non-bold but with the same notation $\mathscr{M}_0(\mathbf{u})$. $\mathscr{M}_0(\mathbf{u})$ vanishes at a free surface. See Takeuchi & Saïto (1972) and Woodhouse & Dahlen (1978) for more details.

3 1-D EXAMPLE

Let us first illustrate in a 1-D example the impact of a radiation boundary on the normal-mode properties and normal-mode summation techniques. We will take the simple wave equation

$$\frac{\partial^2 u}{\partial t^2} - c^2\frac{\partial^2 u}{\partial x^2} = 0, \tag{5}$$

where c is the velocity. We take a semi-infinite tube with a first finite part of length L, which will be described as a cavity, in contact with an infinite half-space starting at $x=L$, and assume a rigid boundary at the origin $x=0$ (see Fig. 1). c_1, c_2 and ρ_1, ρ_2 are the velocities and densities of the left and right parts, respectively, of the tube. Let us now put a source in the left part and

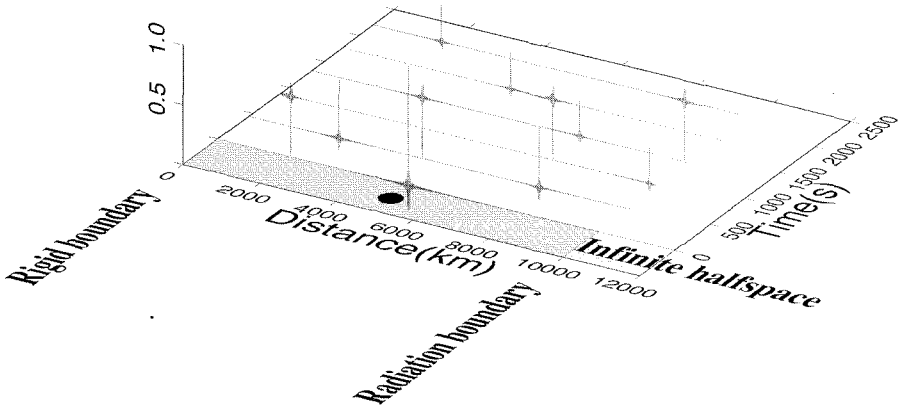

Figure 1. 1-D example of a radiating boundary condition located at the right side of the figure ($x=10\,000$ km). The geometry is shown at the front of the figure. There is a rigid boundary on the left-hand side ($x=0$ km). The velocity and the density are 6000 m s^{-1} and 3000 kg m^{-3} in the cavity. Both the velocity and density are reduced by two in the infinite medium located on the right-hand side, so that the reflection coefficient is 3/5. Six snapshots are shown, each separated by 220 s, the first starting at the initial time. The source is a Dirac delta function source, located in the middle of the 10 000-km-long line. The snapshots are constructed by summing the first 1000 normal modes and by using relation (17) for the normalization.

therefore in the cavity. Waves launched in the first part reflect at the discontinuity $x=L$, with a reflection coefficient equal to $(\rho_1 c_1-\rho_2 c_2)/(\rho_1 c_1+\rho_2 c_2)$. Part of the signal will be transmitted to the infinite part, with the non-zero amplitude transmission coefficient equal to $(2\rho_1 c_1)/(\rho_1 c_1+\rho_2 c_2)$.

From the boundary-condition point of view, this corresponds to an open boundary condition of the cavity at $x=L$. At $x=L^+$ (the right, infinite side of the discontinuity), the propagation is towards the right only, and this boundary condition is therefore

$$\frac{\partial u}{\partial t}(L^+)+c_2\frac{\partial u}{\partial x}(L^+)=0. \tag{6}$$

Such a new boundary condition induces a severe mathematical impact on the structure of the wave operator. Let u and v be two displacement fields and let us write the integral form of the elastic operator as

$$\begin{aligned}(v|Au)&=-\int_0^L dx\, v^*\,\rho_1 c_1^2\frac{\partial^2 u}{\partial x^2}\\&=\int_0^L dx\,\rho_1 c_1^2\frac{\partial v^*}{\partial x}\frac{\partial u}{\partial x}+i\omega\rho_2 c_2[u\,v^*]_{x=L}\\&=(v|A_0u)+(v|\delta Au),\end{aligned} \tag{7}$$

where * denotes the complex conjugate and where we have used the boundary condition (6) and the continuity of stress at $x=L$. The first part, A_0, is the Hermitian, positive-defined operator, as obtained for a cavity with a free or rigid surface at $x=L$. The difference δA is associated with the open boundary condition. In fact, it breaks the Hermitian structure of the operator A. It is, however, important to note that the operator A is frequency-dependent but still symmetric when the bracket product is defined without the complex conjugation:

$$\begin{aligned}\langle v|Au\rangle&=-\int_0^L dx\, v\,\rho_1 c_1^2\frac{\partial^2 u}{\partial x^2}\\&=\int_0^L dx\,\rho_1 c_1^2\frac{\partial v}{\partial x}\frac{\partial u}{\partial x}+i\omega\rho_2 c_2[u\,v]_{x=L}\\&=\langle v|A_0u\rangle+\langle v|\delta Au\rangle.\end{aligned} \tag{8}$$

This operator therefore has properties that are identical to those of an anelastic operator, which makes sense from a physical point of view because both the attenuation and the open boundary condition lead to the escape of the seismic energy from the cavity (into the infinite medium in our case; into heat for anelasticity). Therefore, the theory of normal-mode summation techniques developed by Lognonné (1989), recalled by Tromp & Dahlen (1990) in the non-rotating anelastic case, and generalized by Lognonné (1991) in the more general case of an anelastic rotating earth can be used. We will show later that this is also valid for the 3-D case; see Lognonné (1991) for a more detailed description.

As in the case of Lognonné (1991), such a symmetric frequency-dependent operator will yield a new orthogonality relation between modes, called the bi-othogonality relation. In our example, we can express it by starting from two modes u_1 and u_2 and their

associated eigenfrequencies ω_1 and ω_2, both satisfying the normal-mode equation with two different frequencies:

$$\omega_1^2 u_1 = -c_1^2 \frac{\partial^2 u_1}{\partial x^2}\,, \tag{9}$$

$$\omega_2^2 u_2 = -c_1^2 \frac{\partial^2 u_2}{\partial x^2}\,. \tag{10}$$

We multiply eqs (9) and (10) by $\rho_1 u_2$ and $\rho_1 u_1$ respectively, integrate over L and take the difference. By using the continuity of stress and the boundary condition, we finally obtain a bi-orthogonality relation:

$$\int_0^L dx\, \rho_1 u_1(x) u_2(x) - i\rho_2 c_2 \frac{u_1(L) u_2(L)}{\omega_1 + \omega_2} = 0\,. \tag{11}$$

We see here that the non-free surface destroys the classical orthogonality relation of modes for the case with a free or rigid surface at $x = L$. We now search the normal modes $u_n(x)$ and their eigenfrequency ω_n. Due to the loss of energy at each reflection, normal modes have complex frequencies. However, they can be found by using the boundary equations and the wave equation. From the latter, the rigid boundary at $x = 0$ and the continuity of displacement at $x = L$ and the radiation boundary at $x = L^+$, it is easy to show that the normal modes must have the following general expressions:

$$u(x) = \frac{e^{ik_1 x} - e^{-ik_1 x}}{e^{ik_1 L} - e^{-ik_1 L}}\,, \qquad \text{for } x \leq L\,, \tag{12}$$

$$u(x) = \frac{e^{-ik_2 x}}{e^{-ik_2 L}}\,, \qquad \text{for } x \geq L\,, \tag{13}$$

where $k_1 = \omega/c_1$, $k_2 = \omega/c_2$. The expression of the mode in the right, infinite part of the tube results directly from the dispersion relation and boundary equation (6). The continuity of the stress yields the characteristic equation defining the eigenfrequency:

$$e^{2ik_1 L} = \frac{\rho_2 c_2 - \rho_1 c_1}{\rho_2 c_2 + \rho_1 c_1}\,, \tag{14}$$

which gives the eigenfrequencies, expressed as

$$\frac{\omega_n}{c_1} = \left(n + \frac{\epsilon}{2}\right)\frac{\pi}{L} - \frac{i}{2L} \ln\left|\frac{\rho_1 c_1 - \rho_2 c_2}{\rho_2 c_2 + \rho_1 c_1}\right|\,, \tag{15}$$

where $\epsilon = 0$ for $\rho_2 c_2 > \rho_1 c_1$, $\epsilon = 1$ for $\rho_2 c_2 < \rho_1 c_1$ and n is the mode number. Note that $\omega_n = -\omega^*_{-n-\epsilon}$ and that $u_n(x) = u^*_{-n-\epsilon}$, where * denotes the complex conjugate. As shown by Lognonné (1991), modes must be normalized by using the bi-orthogonality condition, and therefore must satisfy

$$\int_0^L dx\, \rho_1 u_n^2(x) - i\rho_2 c_2 \frac{u_n^2(L)}{2\omega_n} = 1\,. \tag{16}$$

Seismograms can then be computed by normal-mode summation. For the example shown here, the solution to our example for an initial displacement given by a Dirac delta function at $x = L/2$ is

$$u(x, t) = \sum_{n=-\infty}^{n=+\infty} u_n(x) u_n(L/2) e^{i\omega_n t}\,. \tag{17}$$

The summation is explicitely real, due to the relation between modes of indexes n and $-n-\epsilon$, and the normalization of the modes is carried out with relation (16). The results of this summation are shown in Fig. 1 for different times. It is clearly seen that the imperfect reflection is well modelled by the normal-mode summation. Fig. 2 shows the error in the normal mode summation when the relation (17) is used but with modes normalized with only the left part of relation (16).

4 CASE OF A PLANET WITH ATMOSPHERE

We now consider the 3-D spherically symmetric case and the normal-mode equation in the atmosphere. As for the 1-D case, we need to express the wave equation with a boundary condition for upward radiation at the top of the atmosphere. Following Takeuchi & Saïto (1972), we know that in a spherical earth the spheroidal normal modes are decoupled from the toroidal normal modes and, in

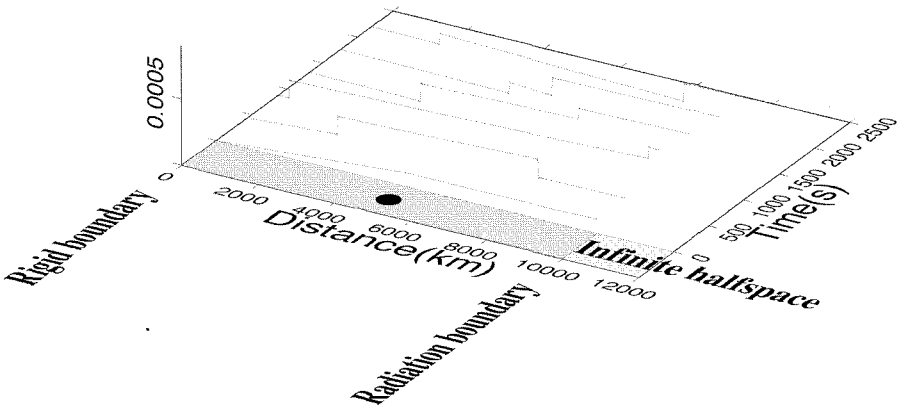

Figure 2. Same as Fig. 1 but for the error caused by the normal-mode summation when the modes are normalized without the right part of eq. (16). The residual is small but is associated with a non-causal step between the two propagating packets. Note, however, that the modes are the complex modes.

fluid areas, are the solution of the propagator

$$\frac{d}{dr}\begin{pmatrix} Y_1 \\ Y_2 \\ Y_5 \\ Y_6 \end{pmatrix} = \mathbf{B}\begin{pmatrix} Y_1 \\ Y_2 \\ Y_5 \\ Y_6 \end{pmatrix}. \tag{18}$$

Here, the functions $Y_1 = U$ and $Y_2 = -P$ are related to the vertical displacement U and the Lagrangian pressure perturbation P. Y_5 is the mass redistribution potential, Y_6 is another function related to the mass redistribution, and $\mathbf{B}$ is the propagator matrix, which depends on the model, the radius r, the frequency ω and the angular order ℓ of the mode. Y_3 and Y_4 are not used in the fluid parts, and the horizontal displacement U_h is obtained from the definition of the pressure fluctuation:

$$P(\mathbf{u}) = -\kappa \boldsymbol{\nabla} . \mathbf{u} = -\kappa\left(2\frac{U}{r} + \frac{\partial U}{\partial r} - \ell(\ell+1)\frac{U_h}{r}\right), \tag{19}$$

where κ is the bulk modulus. As a consequence of the rapid variation of the element of matrix $\mathbf{B}$ in the atmosphere, related to the exponential decay of the density and compression modulus, it is preferable to rewrite eq. (18) in the atmosphere using new variables. Among the possible methods (Unno *et al.* 1989; Watada 1995), we choose a renormalization technique for the density (Lognonné & Romanowicz 1990) and use the variables

$$\begin{aligned} \tilde{Y}_1 &= r\sqrt{\rho g}\, Y_1, \\ \tilde{Y}_2 &= \frac{r}{\sqrt{\rho g}}\, Y_2, \\ \tilde{Y}_5 &= \frac{\sqrt{\rho g}}{4\pi \mathscr{G}}\, Y_5, \\ \tilde{Y}_6 &= \frac{\sqrt{\rho g}}{4\pi \mathscr{G}}\, Y_6, \end{aligned} \tag{20}$$

where $\mathscr{G}$ is the gravitation constant, ρ is the density and g is the gravity. All four variables have the same dimensions, and the propagator can now be rewritten as (see Appendix A for details)

$$r\frac{d}{dr}\begin{pmatrix} \tilde{Y}_1 \\ \tilde{Y}_2 \\ \tilde{Y}_5 \\ \tilde{Y}_6 \end{pmatrix} = C\begin{pmatrix} \tilde{Y}_1 \\ \tilde{Y}_2 \\ \tilde{Y}_5 \\ \tilde{Y}_6 \end{pmatrix}, \tag{21}$$

where the non-dimensional matrix C is given by

$$C=\begin{bmatrix} -\left(1+\frac{K}{2}\right)+\frac{\ell(\ell+1)g}{\omega^2 r} & \frac{gr}{c^2}-\frac{\ell(\ell+1)g}{\omega^2 r} & 4\pi\mathscr{G}\rho\,\frac{\ell(\ell+1)}{\omega^2} & 0 \\ \frac{\ell(\ell+1)g}{\omega^2 r}-4-\frac{\omega^2 r}{g} & \left(1+\frac{K}{2}\right)-\frac{\ell(\ell+1)g}{\omega^2 r} & 4\pi\mathscr{G}\rho\left(\frac{\ell(\ell+1)}{\omega^2}-(\ell+1)\,\frac{r}{g}\right) & \frac{4\pi\mathscr{G}\rho r}{g} \\ -1 & 0 & \frac{4\pi\mathscr{G}\rho r}{g}+\frac{K}{2}-3-\ell & 1 \\ -(\ell+1)+\frac{\ell(\ell+1)g}{\omega^2 r} & -\frac{\ell(\ell+1)g}{\omega^2 r} & \frac{4\pi\mathscr{G}\rho\ell(\ell+1)}{\omega^2} & \ell-2+\frac{K}{2}+\frac{4\pi\mathscr{G}\rho r}{g} \end{bmatrix}. \tag{22}$$

In this equation, K is defined as the non-dimensional inverse of the scale height of ρg:

$$K=-r\,\frac{d\ln[(\rho g)/(\rho_0 g_0)]}{dr}, \tag{23}$$

where ρ_0 and g_0 are the density and gravity at an arbitrary altitude and c is the acoustic velocity. Typically, in the middle and lower atmosphere, the scale height is between 6.5 and 8.5 km and the density is about 1.22 kg m^{-3} at zero altitude. For a frequency of 5 mHz, the terms $g/(\omega^2 r)$, $(gr)/c^2$, $(4\pi\mathscr{G}\rho)/\omega^2$, $(4\pi\mathscr{G}\rho)/g$ and K are of the order of 10^{-3}, 600, 10^{-6}, 10^{-10} and 5×10^{7}, respectively. All the terms of the matrix C are now slowly varying with altitude and the matrix is dominated by the diagonal terms $K/2$.

We now consider the case of an open radiating surface and take eq. (21) at the top of the atmosphere, where the density is close to 0. The non-gravity terms $\tilde{Y}_1$ and $\tilde{Y}_2$ are then decoupled from the gravity terms $\tilde{Y}_5$ and $\tilde{Y}_6$ and we have

$$r\,\frac{d}{dr}\begin{pmatrix}\tilde{Y}_1\\ \tilde{Y}_2\end{pmatrix}=\begin{bmatrix} -\left(1+\frac{K}{2}\right)+\frac{\ell(\ell+1)g}{\omega^2 r} & \frac{gr}{c^2}-\frac{\ell(\ell+1)g}{\omega^2 r} \\ \frac{\ell(\ell+1)g}{\omega^2 r}-4-\frac{\omega^2 r}{g} & \left(1+\frac{K}{2}\right)-\frac{\ell(\ell+1)g}{\omega^2 r} \end{bmatrix}\begin{pmatrix}\tilde{Y}_1\\ \tilde{Y}_2\end{pmatrix}. \tag{24}$$

Following Unno *et al.* (1989) and Watada (1995), we will assume that at the top of the model, the dependent variables $\tilde{Y}_1$ and $\tilde{Y}_2$ are functions of r and depend locally on the radius as r^λ, so that λ is the solution of the characteristic equation

$$\det\begin{bmatrix} C_{11}-\lambda & C_{12} \\ C_{21} & -C_{11}-\lambda \end{bmatrix}=0, \tag{25}$$

where C_{11}, C_{12} and C_{21} are three elements of the matrix (24), all depending on the frequency and det is the determinant of the matrix. Our characteristic equation is similar to that of Watada (1995), but is more symmetric due to the density renormalization. As shown in Appendix B, the solutions of this characteristic equation are $\lambda=\pm\Delta$. Δ is complex and depends on the frequency; its expression is given in Appendix B. Real roots mean a trapped mode, and imaginary roots upward or downward propagation. We know, on the other hand, that the energy density E of a normal mode is proportional to

$$E\propto\rho\omega^2(U^2+U_h^2)\propto\frac{\omega^2\tilde{Y}_1^2}{r^2 g}\propto r^{\pm\Delta}\propto \mathrm{e}^{\pm z(\Delta/r_s)}, \tag{26}$$

where z is the altitude above the solid/atmosphere boundary located at r_s. The type of solution is controlled by two cut-off frequencies ω_1 and ω_2, which are given in Appendix B. For frequencies $\omega_1\le\omega\le\omega_2$, Δ is real, and we have two solutions with either growing or decreasing energy density. The decaying case corresponds to leaky modes. For frequencies $\omega_2\le\omega$ or $\omega\le\omega_1$, Δ is purely imaginary and we have an acoustic or gravity mode, respectively, with upward or downward phase velocity.

When the sources are assumed inside the Earth or atmosphere, only the eigenvalue corresponding to trapped modes or upward-propagating acoustic modes is chosen. With this eigenvalue λ, we obtain from eq. (24) the new boundary condition for the 'open' case:

$$\mathscr{M}_1(\mathbf{u})=P(\mathbf{u})-\frac{C_{11}-\lambda}{C_{12}}\,\rho g U=0, \tag{27}$$

instead of the zero-pressure free boundary condition, where U is the vertical component of the mode $\mathbf{u}$ and we recall that C_{11}, λ and C_{12} depend on the frequency. This new boundary condition can then be used for the expression of the elastodynamic operator $\mathbf{A}$ in

variational form. We then have, by integration of the right side of the dot product of eq. (1) by a displacement vector $\boldsymbol{v}$,

$$\begin{aligned}\langle \boldsymbol{v}|\mathbf{A}(\mathbf{u})\rangle &= \int_{\mathscr{V}} d^3r\, \rho\, \boldsymbol{v}\,.\,\mathbf{A}(\mathbf{u}) \\ &= \int_{\mathscr{V}} d^3r\, (\nabla \boldsymbol{v} : \mathbf{T}_{\text{elastic}} + \boldsymbol{v}\,.\,(\nabla(\mathbf{u}\,.\nabla \mathbf{T}_0) + \operatorname{div}(\rho\mathbf{u})\mathbf{g} + \rho\nabla\Phi_{E_1})) - \int_{\Sigma} d\Sigma\, \boldsymbol{v}\,.\mathbf{T}_{\text{elastic}}\,.\,\mathbf{n}\,,\end{aligned} \tag{28}$$

where $\mathscr{V}$ is the integration volume and d^3r is the integration weight. The term with a surface integral can be written using the boundary condition, but does not vanish for the 'open boundary condition'. It expresses the perturbation related to the new boundary condition, and can be written as

$$\langle \boldsymbol{v}|\delta\mathbf{A}(\mathbf{u})\rangle = -\int_{\Sigma} d\Sigma\, \boldsymbol{v}\,.\mathbf{T}_{\text{elastic}}\,.\,\mathbf{n} = \int_{\Sigma} d\Sigma\, V\, P(\mathbf{u}) = \frac{C_{11}-\lambda}{C_{12}} \int_{\Sigma} d\Sigma\, \rho g\, U\, V\,, \tag{29}$$

where we have used the boundary condition (27), and U and V are the vertical components of $\mathbf{u}$ and $\boldsymbol{v}$ respectively. The operator $\mathbf{A}$ can finally be written as

$$\mathbf{A} = \mathbf{A}_0 + \delta\mathbf{A}\,, \tag{30}$$

where $\mathbf{A}_0$ is the free boundary operator, expressed as in relation (28), but without the surface integral, and $\delta\mathbf{A}$ is the surface integral, which vanishes for a free boundary condition and is given by relation (29) for the open boundary condition. Note that, as in the 1-D example, $\mathbf{A}$ remains symmetric, but is no longer Hermitian and is now frequency-dependent through $\delta\mathbf{A}$. It has properties comparable to those of an anelastic operator, and the theory developed by Lognonné (1991) for seismogram summation can be used.

5 MAPPING

Let us now compute the normal modes of the problem. With respect to the classical elastic case, we have two major differences. The first is related to the boundary condition, which is frequency-dependent, and therefore we need an iterative process where the computed eigenfrequency is reinjected into the boundary condition at each step. The second is related to the fact that, even for a purely elastic model, modes will not be trapped and will therefore have both complex frequency and amplitude. These two effects cannot be treated by most normal-modes software using the minor methods (Woodhouse 1988). Such software is, however, well adapted, assuming an external free surface, to the computation for planets with atmosphere [see Lognonné *et al.* (1994) for an application to Jupiter, and Lavely & Ritzwoller (1992) for an application to the Sun].

Watada (1995) developed another shooting method where the equations are integrated from a starting level. Such a method ends up with a characteristic equation, the solution of which gives the eigenfrequencies. It is possible to account for the open boundary conditions, but this is complex due to its frequency dependence. The computation therefore becomes iterative and slowly convergent, unless a good guess of the eigenfrequency is made for the first iteration. Watada (1995) therefore used this method to compute mostly the normal modes of the earth/atmosphere system with free or rigid boundary conditions, and only a few modes with the open boundary condition.

We choose in this paper a variational Rayleigh–Ritz method, as described by Aki & Richards (1980), for example. Such a method will be able to handle the strong perturbation of the operator in the mode computation, contrary to perturbation theories. As with all variational methods, it is based on the use of a set of basis functions, on which the solutions are projected. All these basis functions must therefore satisfy the boundary conditions, including relation (27), and must constitute a complete basis. Moreover, it is numerically highly desirable to use functions that minimize the truncation error when a finite subset of the basis is used instead of the formal infinite set. A natural way to minimize such an error is to use a set of basis functions that are as close as possible to the expected solutions. With such a basis, and for a given angular order ℓ, any solution of the problem $\boldsymbol{v}$ is expected to be of the form

$$\boldsymbol{v} = \sum_n c_{n\,n}\boldsymbol{v}_\ell\,. \tag{31}$$

To determine such a basis, we start from the SNREI-FB (spherical, non-rotating, elastic, isotropic, free boundary) normal-mode functions, denoted ${}_n\mathbf{u}_\ell$, that are solutions of eq. (21) for a model including the solid earth and the atmosphere, but with a free boundary at the top of the atmosphere. Such functions form a complete basis, and are therefore potential candidates for the variational basis functions. Moreover, even for a completely different boundary condition in the atmosphere, the modes with most of their energy in the solid earth will show only slight perturbations in the solid earth with respect to the SNREI-FB modes. This will also be partially true for all modes trapped in the atmosphere. However, these modes satisfy the free-surface

boundary condition

$$\mathcal{M}_0({}_n\mathbf{u}_\ell) = P({}_n\mathbf{u}_\ell) = 0\,, \tag{32}$$

and we need to transform these functions into new functions satisfying the open boundary condition. We define such a transformation, which will map a function $\mathbf{u}$ with free boundary conditions into a new function $\mathbf{u}'$ with open boundary conditions. Such a transformation must take place only in the atmosphere, and therefore $\mathbf{u}' = \mathbf{u}$ in the solid earth. We first consider the vertical displacement U and the pressure P of $\mathbf{u}$, their corresponding variables $\tilde{Y}_1$ and $\tilde{Y}_2$, the vertical displacement U' and the pressure P' of $\mathbf{u}'$, and their corresponding variables $\tilde{Y}_1'$ and $\tilde{Y}_2'$. $\tilde{Y}_1' = \tilde{Y}_1$ and $\tilde{Y}_2' = \tilde{Y}_2$ in the solid earth. At the bottom of the atmosphere, because of the low atmospheric density, we have

$$r\partial_r \tilde{Y}_1 \approx C_{11}\tilde{Y}_1 + C_{12}\tilde{Y}_2\,. \tag{33}$$

At the top of the atmosphere, if $\mathbf{u}'$ satisfies the open boundary condition, and from relation (25), we have

$$r\partial_r \tilde{Y}_1' = \lambda \tilde{Y}_1'\,. \tag{34}$$

We therefore construct $\tilde{Y}_1'$ from $\tilde{Y}_2$ using the differential equation

$$r\partial_r \tilde{Y}_1' = [C_{11} + f(r)(\lambda - C_{11})]\tilde{Y}_1' + C_{12}\tilde{Y}_2\,, \tag{35}$$

where $f(r) = (r - r_s)/(r_a - r_s)$; r_s and r_a are the radii of the base and top of the atmosphere respectively, and the initial value at the base of the atmosphere is $\tilde{Y}_1$ due to the continuity relations. Note that $f(r) = 0, f(r) = 1$ at the base and top of the atmosphere respectively. Note that $\tilde{Y}_2$ acts as a forcing term in relation (35). From the determination of $\tilde{Y}_1'$, we then fix $\tilde{Y}_2'$ such that the first line of eq. (24) is satisfied:

$$r\partial_r \tilde{Y}_1' = C_{11}\tilde{Y}_1' + C_{12}\tilde{Y}_2'\,, \tag{36}$$

and we then fix the horizontal displacement of $\mathbf{u}'$ such that the constitutive relation between pressure and displacement (19) is verified. When applied to the SNREI-FB modes, ${}_n\mathbf{u}_\ell$, such a mapping will determine a set of new functions, ${}_n\boldsymbol{v}_\ell$, that satisfy explicitly the open boundary condition at the top of atmosphere where the free boundary conditions are satisfied for SNREI-FB, and will verify eq. (19) and the first line of eq. (24).

The main task of the variational method will then be to force the solution, expressed as a finite summation of these basis functions ${}_n\boldsymbol{v}_\ell$, to solve also the second line of eq. (24). This, however, implies that this set of functions is a complete basis. Appendix C shows that this is the case when the basis of the kernel of $\mathcal{M}$ is added (for example, functions inducing zero pressure in the atmosphere, such as secular atmospheric motions) and when all modes of the initial model are used; that is, seismic spheroidal modes, ${}_nS_\ell$, and acoustic modes, ${}_nP_\ell$, with most of their energy in the solid–liquid earth and atmosphere respectively, and also gravity modes, either from the liquid core or from the atmosphere. In our numerical example, we will not consider any gravity modes in the set of functions ${}_n\mathbf{u}_\ell$. Also, we will not consider any functions of the kernel of $\mathcal{M}$. The mapping will therefore be limited to the seismic and acoustic modes ${}_n\mathbf{u}_\ell$ of the model with a free boundary at the top of the atmosphere. Such an assumption will probably limit our method to the computation of small-scale atmospheric waves (e.g. infrasounds) and seismic waves, and will exclude medium- and large-scale atmospheric gravity waves, which have periods from about 15 min to longer than 3 hr, and phase velocities of about 100 to 1000 m s^{-1}.

In all our numerical examples, the integration was performed upwards, with a second-order predictor–corrector integration scheme. The horizontal component was then obtained using eq. (19).

The functions obtained can then be used to formulate the variational problem. For each normal mode with angular order ℓ, the computation was performed iteratively for all radial orders n. First, the set of functions ${}_{n'}\boldsymbol{v}_\ell$ with the same angular order but with different radial numbers were obtained after mapping at the frequency of the mode in the free boundary condition ω_0. Here n' was taken in the range sup(0, $n - Nc$), max($n + Nc$, 2^*Nc), where 2^*Nc was the number of basis functions used. The solution, for each n and ℓ value, is then expressed as a summation of these functions:

$$\boldsymbol{v} = \sum_{n'} c_{n'n'}\boldsymbol{v}_\ell\,, \tag{37}$$

where the indices n, ℓ are omitted in $\boldsymbol{v}$ and $c_{n'}$ for simplicity. This form was then used to find the normal mode, for example the coefficients c_n' of (37). We start from

$$-\omega^2\boldsymbol{v} = -\mathbf{A}(\omega)\boldsymbol{v}\,. \tag{38}$$

Using a second-order Taylor expansion around the frequency ω_0, we first obtain

$$-\omega^2\boldsymbol{v} = -[\mathbf{A}(\omega_0) + (\omega - \omega_0)\partial_\omega \mathbf{A}(\omega_0) + \frac{1}{2}(\omega - \omega_0)^2\partial_{\omega^2}\mathbf{A}(\omega_0)]\boldsymbol{v}\,, \tag{39}$$

and we can then express the variational problem in matrix form. [See Park & F. Gilbert (1986) for another example of this technique.] We finally obtain the following:

$$\omega\left[1-\frac{1}{2}\,\partial_{\omega^2}A\right]\begin{bmatrix}\omega\boldsymbol{v}\\ \boldsymbol{v}\end{bmatrix}=\begin{bmatrix}\partial_\omega A-\omega_0\partial_{\omega^2}A & A(\omega_0)-\omega_0\partial_\omega A+\dfrac{\omega_0^2}{2}\,\partial_{\omega^2}A\\ 1-\dfrac{1}{2}\,\partial_{\omega^2}A & 0\end{bmatrix}\begin{bmatrix}\omega\boldsymbol{v}\\ \boldsymbol{v}\end{bmatrix}. \tag{40}$$

The solution with the eigenfrequency nearest the starting frequency was computed with classical eispack routines (Smith *et al.* 1976). Note that the expression of Liu *et al.* (1976) for the frequency dependence of the solid earth velocities and quality factor was taken, and the imaginary part of the normal modes was therefore also computed in the solid parts. The process was then iterated by updating the frequency ω_0 with the computed frequency until convergence. Note, however, that in matrix form, and due to the fact that the basis is not orthogonal, the identity matrix is dense, with non-zero terms between all modes with the same ℓ and m, but different n.

6 NUMERICAL APPLICATION

We now use the theory detailed above for the computation of the normal mode of the Earth. We use the anisotropic model PREM of Dziewonski & Anderson (1981) and the US Standard atmosphere model (1976) up to an altitude of 150 km. Normal modes are first calculated using the mineos software (Woodhouse 1988) up to 20 mHz. For each angular order and radial order, the normal mode with the free surface is calculated.

The second stage of computation needs, for all angular orders ℓ, to solve the variational problems for all the harmonics. This iterative computation was performed by solving the variational problem (40) using the set of basis functions as described in the previous section. 40 test functions ($Nc=20$) were used; these were initially mapped with the free surface normal-mode eigenfrequency. The size of the eigenproblem was therefore 80×80. After finding the new normal-mode frequency, the new frequency was then used for a new iterative mapping, up to a convergence fixed to a difference criteria. This iteration was terminated when the difference between two successive frequencies was less than 5 per mille.

The convergence of the process was checked with the residual of the second line of eq. (40) in the strong form, and then estimated by the norm of the residual over the norm of the velocity field limited to an integration in the atmosphere. In this weak form, errors after one or two iterations for the solid Earth normal modes and after a few iterations for the atmospheric modes are found to be about or less than 0.5 per mille (5×10^{-4}). Tests have shown that the error decreases with the increasing number of modes used in the variational method.

Fig. 3 shows the eigenfrequencies of the atmospheric normal modes, which have most of their energy in the atmosphere. We found that two of these modes are trapped within the atmosphere; they have frequencies of 3.681 and 4.405 mHz, and quality factors

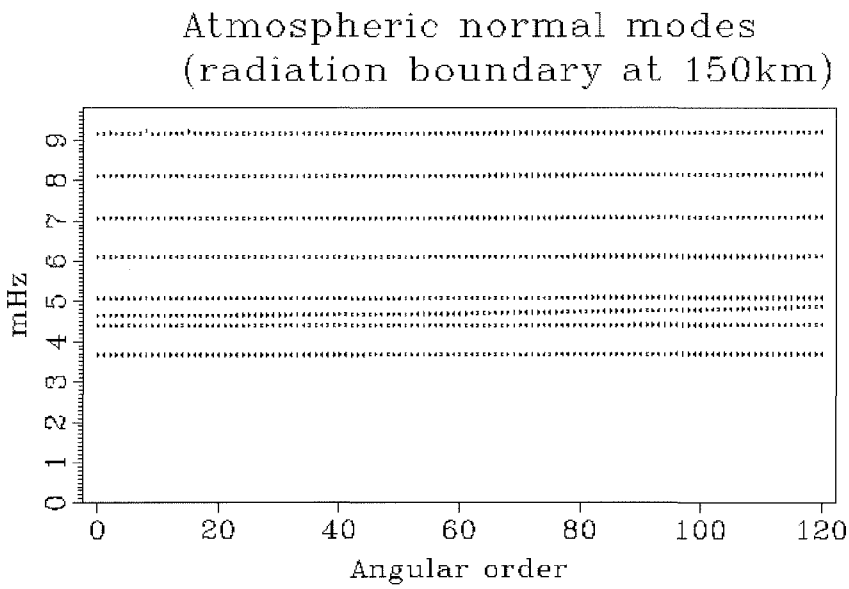

Figure 3. Atmospheric normal-mode frequencies. The model is PREM (for the solid Earth) and US Standard Model (1976) for the atmosphere. Note that the atmospheric modes are associated with a succession of frequencies, for example 3.681, 4.405, 4.696, 5.076, 6.104, 7.067, 8.118 and 9.171 mHz at $\ell=60$ for a boundary condition at 150 km. Horizontal group velocities are very low, between 10 and 15 m s^{-1}, but the third harmonics have a higher group velocity of about 60 m s^{-1}.

of respectively 114.7 and 21.17. For the fundamental modes in particular, these frequencies and Q factors do not change strongly with the position of the boundary condition. The other modes are not trapped and therefore have frequencies and Q factors that depend on the position of the boundary condition. For an altitude of 150 km, we have the following frequencies at $\ell = 60$: 4.696, 5.076, 6.104, 7.067, 8.118 and 9.171 mHz, with Q factors of 2.838, 8.417, 5.954, 6.779, 7.334 and 7.883, respectively. Horizontal group velocities are very low, between 10 and 15 m s^{-1} for all modes at $\ell = 50$ except for the third harmonics, which have a higher group velocity of about 60 m s^{-1}. Note that the first two smaller frequencies are equal or close to quasi-monochromatic oscillations reported from seismic or ionogram data recorded after atmospheric explosions or storms (Table 1).

Figs 4 to 6 show the vertical amplitudes (multiplied by the square root of density) of the fundamental atmospheric mode and the first three overtones for the angular order $\ell = 20$. Note that here, as well as in all of the figures showing mode amplitudes, the modes are normalized as follows:

$$\langle \boldsymbol{v}|\boldsymbol{v}\rangle - \frac{1}{2\omega}\langle \boldsymbol{v}|\partial_\omega \mathbf{A}(\omega)v\rangle = 1\,, \tag{41}$$

Table 1. Report of observations. S are seismic data; I are ionograms.

3.68 mHz	S	Pinatubo eruption, 1991	Kanamori & Mori 1992; Widmer & Zürn 1992; Zürn & Widmer 1996
	S	El Chicon eruption, 1982	Zürn & Widmer 1996
	I	convective storms	Georges 1973
4.44 mHz	S	Pinatubo eruption, 1991	Kanamori & Mori 1992; Widmer & Zürn 1992; Zürn & Widmer 1996
4.8 mHz	I	Convective storms	Georges 1973
5.14 mHz	S	El Chicon eruption, 1982	Zürn & Widmer 1996

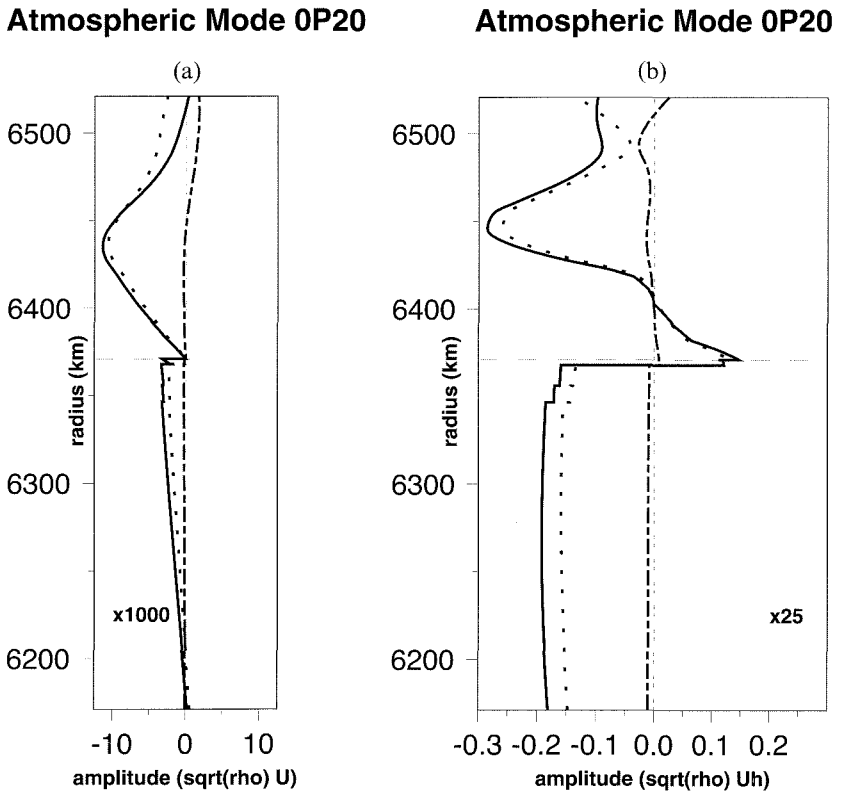

Figure 4. Vertical (a) and horizontal (b) displacement of the fundamental atmospheric mode ${}_0P_{20}$. The amplitudes, multiplied by the square root of density, are plotted, multiplied by 1000 in the solid part for the vertical and by 25 for the horizontal. The solid/atmosphere surface is at 6371 km, just above an oceanic layer of 3 km. The real part of the amplitude is shown as a continuous curve and the imaginary part is a long-dashed curve. The amplitude of the mode computed for a free surface at the top of the atmosphere (150 km altitude) is shown by a dotted curve. Note the strong trapping of the mode, as well as the relatively low amplitude of the imaginary part for both the horizontal and vertical components.

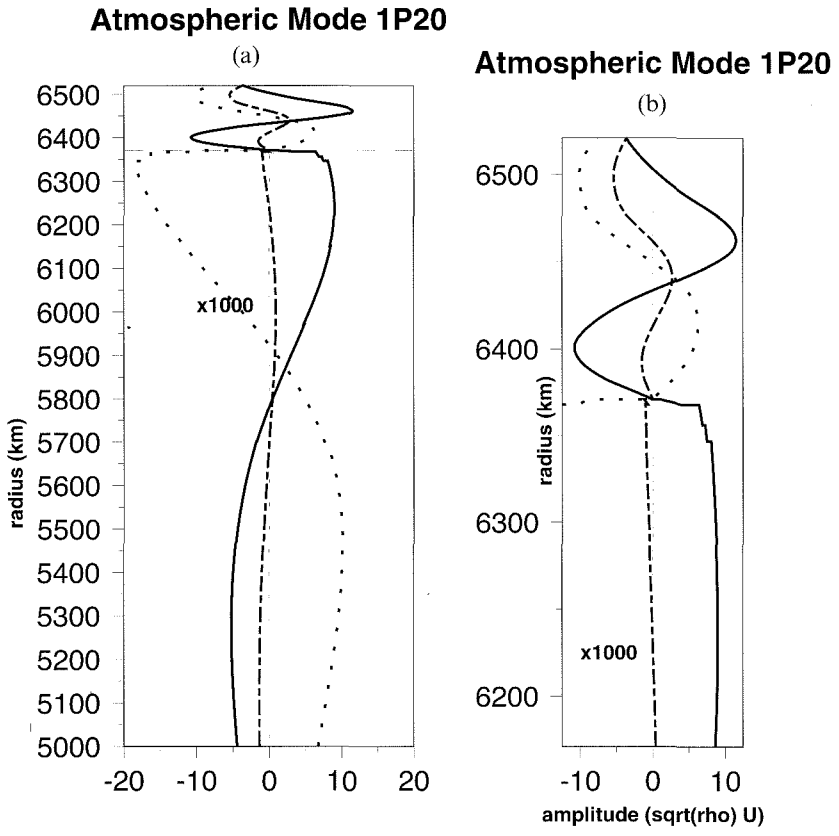

Figure 5. Atmospheric normal modes ${}_1P_{20}$. The vertical amplitude is plotted using the same convention as in Fig. (4). (a) Amplitude between 5000 km and the top of the atmosphere; (b) Close-up of (a) between 6250 km and the top of the atmosphere. Note that the boundary condition strongly reduces the amplitudes in the solid part as a consequence of the lack of reverberation in the atmospheric layer. This mode is less trapped than the fundamental and therefore has a smaller amplitude.

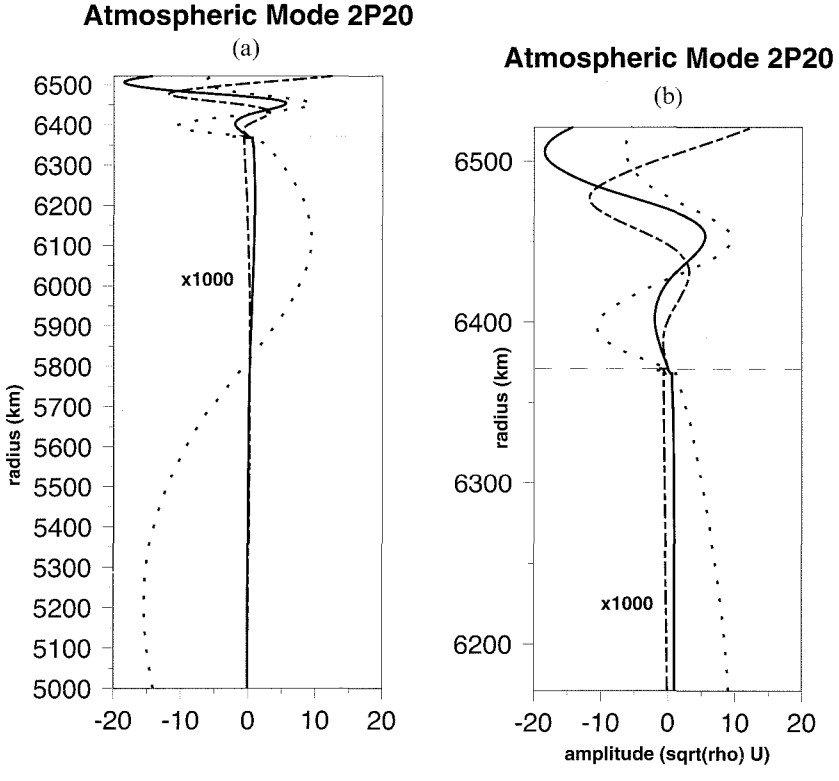

Figure 6. Same as Fig. 5 but for atmospheric normal modes ${}_2P_{20}$. This mode is almost not trapped, and has real and imaginary parts almost in quadrature in the atmosphere.

following eq. (19) of Lognonné (1991), for the same reasons as in the 1-D example of Section 3. The frequency dependence of the operator is expressed by relation (29) for the contribution associated with the radiation boundary condition and by a frequency dependence of the stiffness parameters detailed by Liu *et al.* (1976) for the anelasticity. The amplitudes shown are therefore representative of the amplitudes used for the normal-mode summation. The modes shown in these figures have frequencies of 3.68, 4.40, 4.65 and 5.07 mHz, respectively. Each figure shows the mode computed with a free surface at the top of the atmosphere (dotted curve for the real part), and that with radiation boundary conditions at the top of the atmosphere (solid curve for the real part and long-dashed curve for the imaginary part), here taken at an altitude of 150 km. The smallest perturbation is for the fundamental mode. The fundamental mode is confined in the atmosphere and therefore has a small amplitude at the top of the atmosphere. However, for the first harmonic and in particular for the higher harmonics, the perturbations are very large as a consequence of the lack of confinement of these mode in the atmosphere. The amplitudes in the solid Earth are strongly reduced because of the realistic boundary condition, which suppresses the reverberation between the solid Earth/atmosphere boundary and the top of the atmosphere. This is especially the case for the second and higher harmonics, which have very low Q values. Note also that the imaginary part is comparable to the real part for these modes, another consequence of the lack of trapping. Only the fundamental atmospheric mode is expected to produce significant ground amplitudes far from the source. The very low Q values of the harmonics make their amplitudes significant only near the source.

For the solid Earth normal mode, the perturbations to the frequencies, attenuation and amplitudes in the solid Earth are very small and probably not noticeable. This makes our procedure very efficient, especially as the frequency-dependent mapping does not need to be iterated. Fig. 7 shows the square root of density multiplied by the vertical amplitudes of the fundamental modes ${}_0S_{28}$ ${}_0S_{34}$ ${}_0S_{37}$. An interesting feature is found for the mode ${}_0S_{28}$, which has a frequency very close to the frequency of the first atmospheric mode ${}_0P_{28}$ (3.68 mHz). Its amplitude in the atmosphere is significantly reduced compared to the mode computed with a free boundary condition. As for the atmospheric modes, the efficiency of atmospheric trapping decreases with frequency and the differences between the modes computed for the two boundary conditions increase. The real and imaginary parts of the modes are then almost in quadrature, which indicates an almost upgoing wave.

Fig. 8(a) shows the energy in the atmosphere for the fundamental modes and Figs 9 and 10 are for the first and second overtones. For the fundamental modes, the energy in the atmosphere of the real and imaginary parts of the mode have maxima at $\ell = 28$–29, 34–37 and 42–44, corresponding to frequencies of 3.68, 4.40–4.65 and 5.07 mHz. Below 4.25 mHz, the imaginary part of the

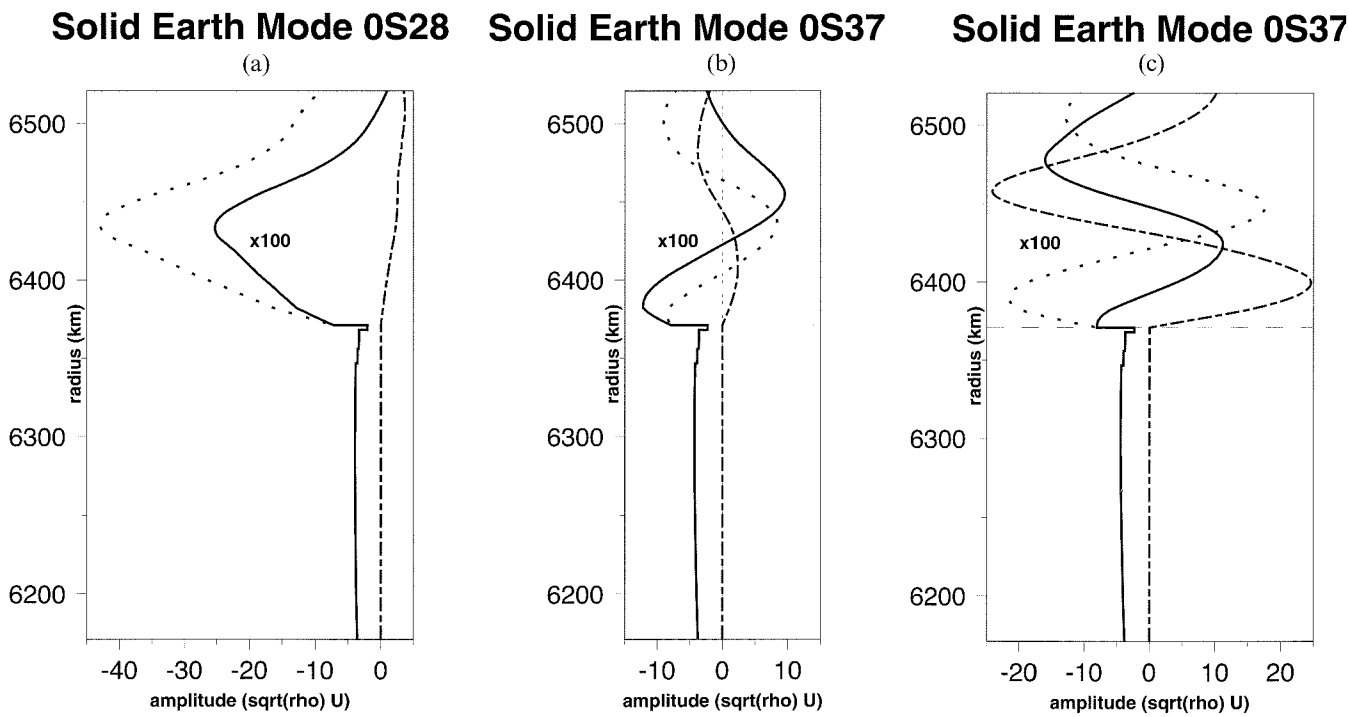

Figure 7. Solid Earth normal modes ${}_0S_{28}$, ${}_0S_{34}$, ${}_0S_{37}$. Same convention as in Figs 4 and 5, but in this case the amplitudes in the atmosphere are multiplied by 100. The frequency of mode ${}_0S_{28}$ is close to the frequency of the atmospheric normal mode, 3.68 mHz. Note, however, that the amplitude of the normal mode with a radiation boundary is reduced by a factor of about 2 compared to the mode computed with a free surface. Mode ${}_0S_{34}$ has a higher frequency, and is associated with an increased imaginary part that is even greater for the mode ${}_0S_{37}$ close to the frequency of the second atmospheric mode, 4.40 mHz. Note also that the imaginary parts are large, almost in quadrature.

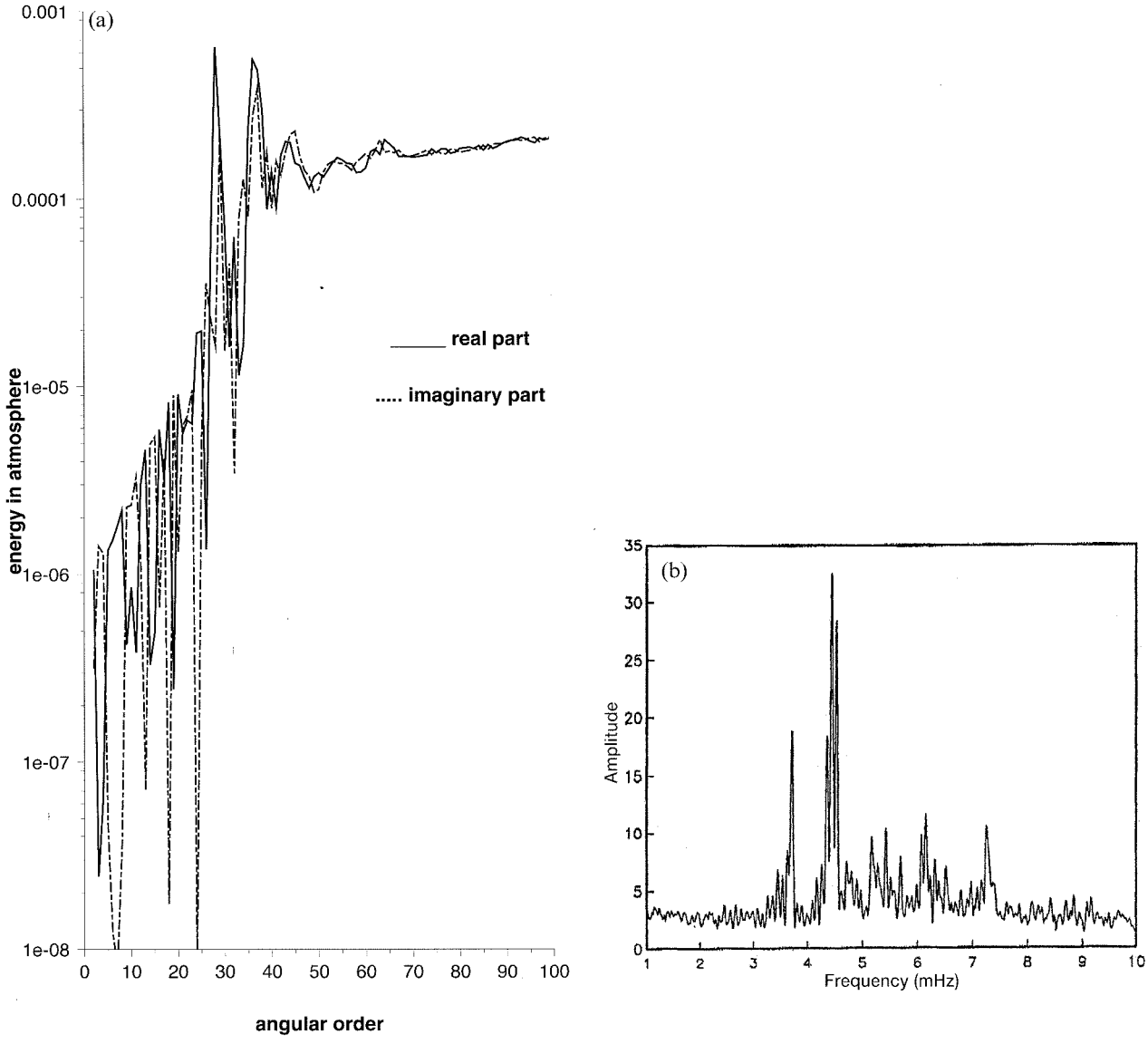

Figure 8. (a) Relative energy of solid Earth fundamental modes in the atmosphere. The continuous curve represents the energy contained in the real part, while the dotted curve is for the imaginary part. The sum of the two curves is the total amount of energy of the mode in the atmosphere. Note the strong resonance at all of the atmospheric characteristic frequencies. Only the mode at 3.68 mHz corresponds to trapped modes, which can be observed far from the source. The peaks at the other frequencies are non-trapped modes, having imaginary parts much higher than the real parts. Note that the relative energy can reach 0.05 per cent, which, for large earthquakes, can be significant for some atmospheric processes. (b) Stacked spectrum of the vertical-component seismograms from the IDA network following the Pinatubo eruption (after Zürn & Widmer 1996). Note the two peaks at 3.68 and 4.40–4.65 mHz. In terms of angular orders, these correspond to $\ell = 28$–29 and 34–37.

amplitude is small, showing the efficiency of atmospheric trapping of modes. At higher frequencies, the real and imaginary parts have comparable amplitudes as a consequence of the lack of trapping. Tests performed for different altitudes of the boundary conditions (150, 200 and 300 km) show almost identical amplitudes below 150 km for such non-trapped modes, demonstrating the efficiency of the method.

Fig. 8(a) can be compared to the observed spectrum obtained for the Pinatubo eruption by Zurn & Widmer (1996), which is shown in Fig. 8(b). The peaks at 3.68 and 4.40–4.65 mHz show that the atmospheric source produced by the Pinatubo eruption excited Rayleigh surface waves only at the few frequencies where energy coupling between the solid Earth and the atmosphere occurs. The secondary peaks at 5, 6 and 7 mHz are dependent on the position of the boundary condition. However, an increase in the thickness of the atmosphere together with the introduction of atmospheric viscosity allow the computation of modes to be relatively insensitive to the boundary conditions (Artru & Lognonné, in preparation). A more precise analysis of the Pinatubo data together with the theory presented here will given in a future paper (Lognonné & Artru, in preparation). Fig. 11(a) shows the square root of

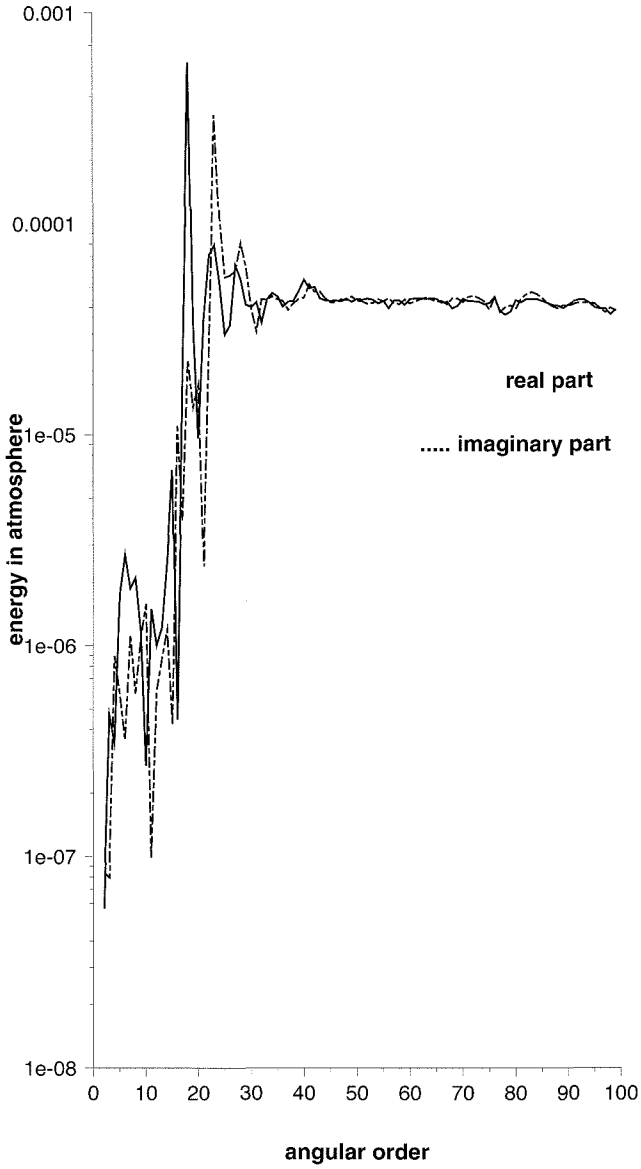

Figure 9. Same as Fig. 8(a) but for the first overtone of solid Earth modes. The constant value is reached when the first harmonics correspond to the Stoneley modes, and are therefore trapped at the CMB.

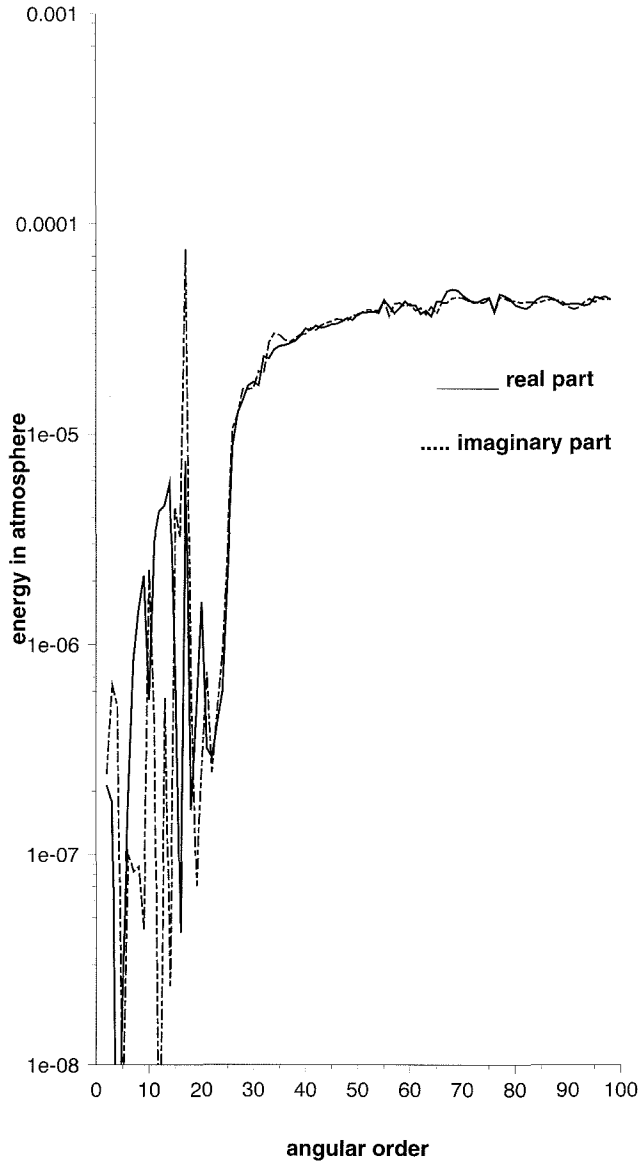

Figure 10. Same as Fig. 8 but for the second overtone of solid Earth modes.

density multiplied by the amplitude of the vertical component of normal modes for the fundamental modes between $\ell = 24$ and 32. The amplitudes increase very strongly near the frequencies of the $\ell = 27$–28 modes, with a maximum of kinetic energy density at an altitude of 60 km, which corresponds to waves trapped in the low-sound-velocity channel located below the thermosphere. Despite a similar amplification, the imaginary parts of the modes (Fig. 11b) have much smaller amplitudes, another consequence of trapping. This is, however, not the case for another window, such as the $\ell = 35$–43 angular order window (Fig. 12). Amplitudes reach a maximum near $\ell = 37$, and the amplitudes of the imaginary parts are comparable. Because these windows are close to those of the fundamental and first harmonic of the atmospheric modes, the modes at $\ell = 27$–28 and at 35–43 have one and two oscillations in the atmosphere, respectively.

A final application of our theory is the computation of seismograms, obtained by summing normal modes. We show here the results of a numerical test, corresponding to an atmospheric explosion at an altitude of 10 km (Fig. 13). The trace shown at the top of the figure is computed by summation of normal modes with a free surface at the top of the atmosphere, while the bottom trace shows the trace with a radiation boundary. On the bottom trace, the artificial reverberations seen on the top trace have been removed and the Rayleigh surface waves are clearly observed.

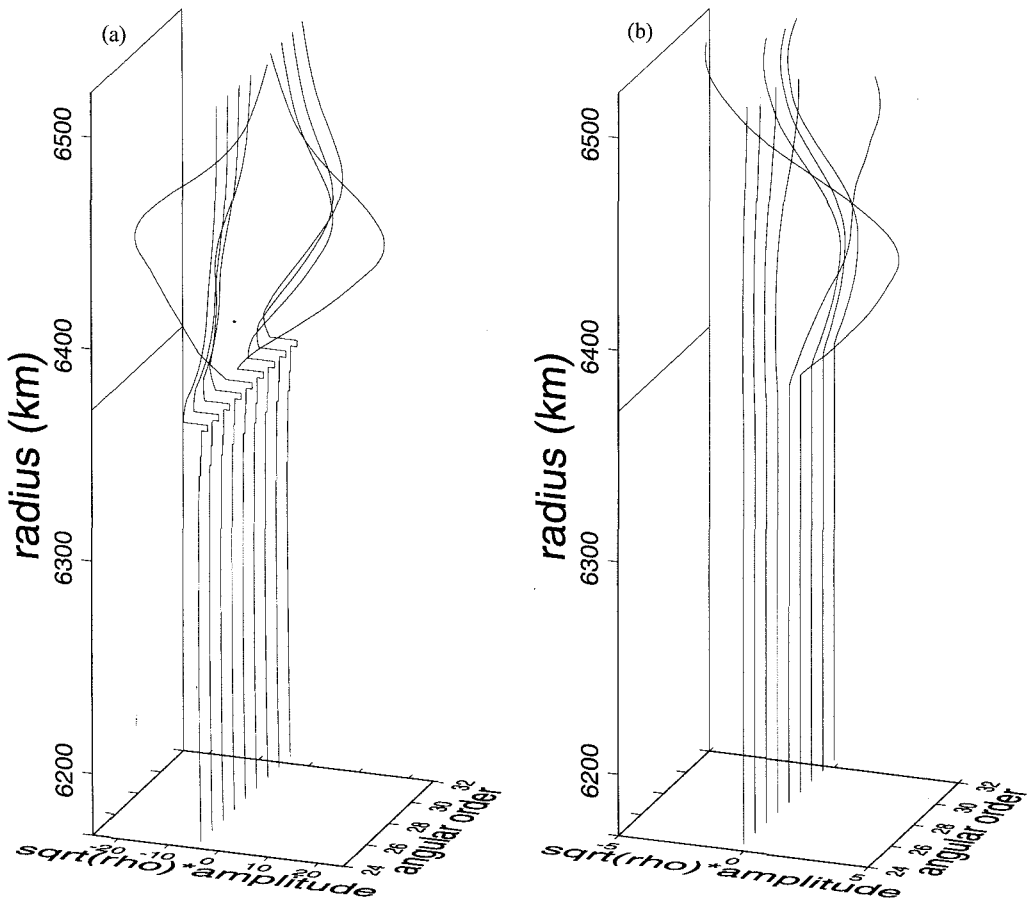

Figure 11. (a) Real part of the solid Earth fundamental modes between $\ell = 24$ and $\ell = 32$. Note the resonance at $\ell = 28$–29, with its associated strong variations in the atmospheric amplitudes. Here the amplitudes in the atmosphere are multiplied by a factor of 100. (b) Amplitudes of the imaginary part at the same scale, showing an equivalent resonance close to $\ell = 28$–29.

7 CONCLUSIONS

Normal modes for the entire Earth, including its atmosphere, have been computed for a proper boundary condition at the top of the atmosphere model to take into account the loss of waves propagating upwards. Such a boundary condition changes the normal-mode properties by making them complex and bi-orthonormal.

Using a mapping technique, we defined a set of basis functions from normal modes computed for a free surface at the top of the atmosphere. These basis functions satisfied the right boundary conditions and defined a complete basis. The normal modes were then approximated by a linear combination of these basis functions and computed by a variational Rayleigh–Ritz method. The spectra found could be separated into solid Earth normal modes and atmospheric normal modes. Except for the fundamental mode, atmospheric modes have low quality factors due to the lack of efficient trapping in the low-sound-velocity atmospheric channel. The two most trapped atmospheric normal modes were found at frequencies of 3.68 and 4.40 mHz. Solid Earth normal modes have large amplitudes in the atmosphere at frequencies close to those of the atmospheric modes. At frequencies higher than 4 mHz, the imaginary parts of the amplitude are almost comparable to the real parts, and cannot be neglected.

These normal modes can be used for computation of seismograms for sources located either in the solid Earth or in the atmosphere, or for computation of the pressure in ionospheric layers generated by earthquakes. Applications of this theory to data will be developed in a future paper.

ACKNOWLEDGMENTS

This is IPGP contribution number 1542 and California Institute of Technology contribution number 8479. We thank Tony Dahlen and an anonymous reviewer for constructive reviews. This work was initiated by PL during a visiting position at the Seismological Laboratory of the California Institute of Technology.

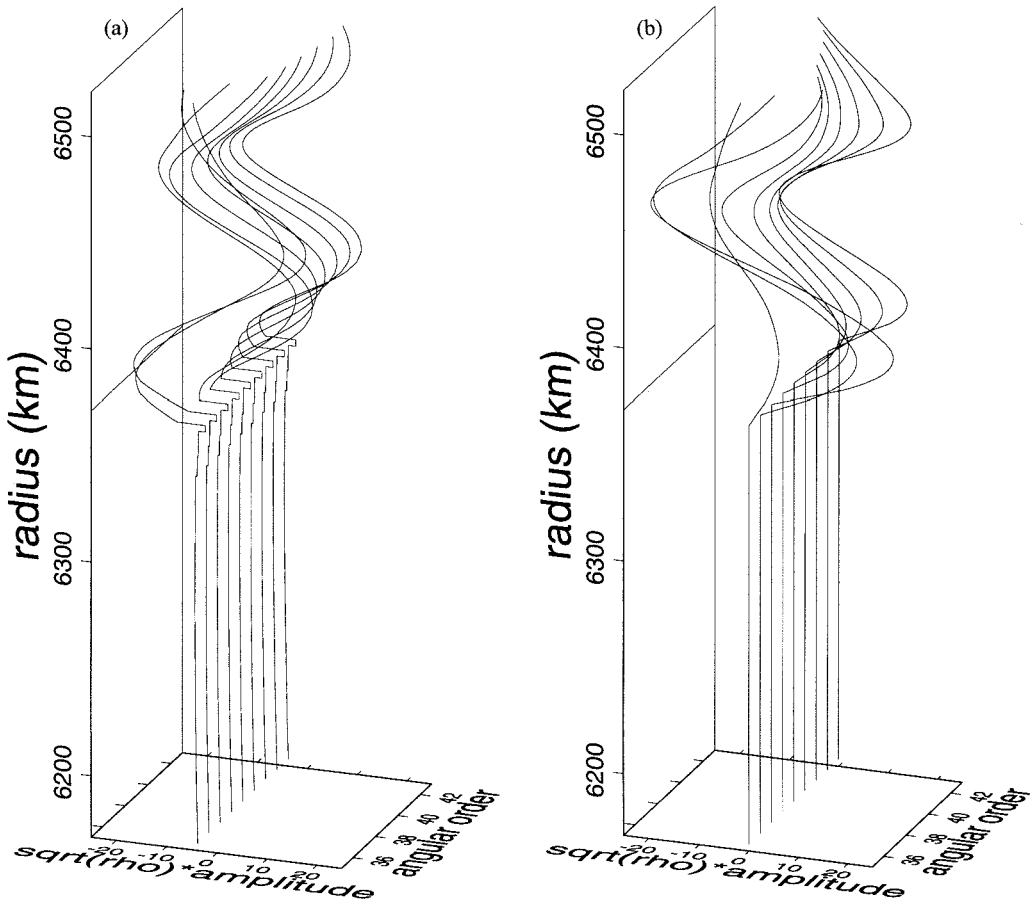

Figure 12. (a) Real part and (b) imaginary part of the solid Earth fundamental modes between $\ell = 35$ and $\ell = 43$. These modes are around the second resonance at 4.40 mHz. Note that the imaginary part has comparable amplitude to the real part.

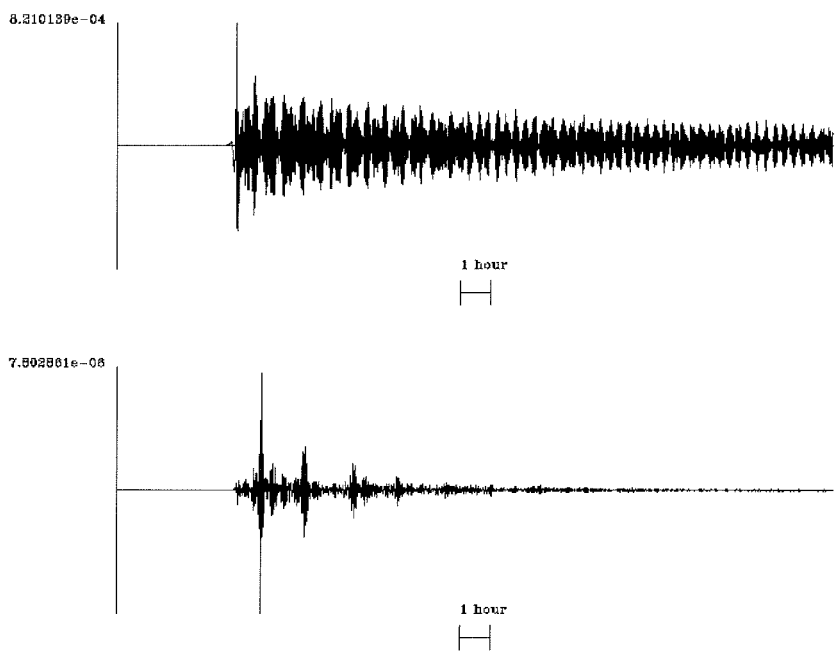

Figure 13. Seismograms computed with an atmospheric top free surface (a) and a radiating boundary (b). All modes with a frequency of less than 10 mHz were summed. The source is an explosion (isotropic point source) at an altitude of 10 km, and the amplitude of the vertical displacement is shown. Unit are metres. The source moment is 10^{17} N m. The receiver is located at an epicentral distance of 95°.

REFERENCES

Aki, K. & Richards, P.G., 1980. *Quantitative Seismology,* Freeman, San Francisco.

Backus, G.E. & Mulcahy, M., 1976a. Moment tensors and other phenomenological descriptions of seismic sources. I. Continuous displacements, *Geophys. J. R. astr. Soc.,* **46,** 341–361.

Backus, G.E. & Mulcahy, M., 1976b. Moment tensors and other phenomenological descriptions of seismic sources. II. Discontinuous displacements, *Geophys. J. R. astr. Soc.,* **47,** 301–329.

Ben-Menahem, A., 1975. Source parameters of the Siberian explosion of June 30, 1908, from analysis and synthesis of seismic signal at four stations, *Phys. Earth planet. Inter.,* **11,** 1–35.

Calais, E. & Minster, J.B., 1995. GPS detection of ionospheric perturbations following the January 17, 1994, Northridge earthquake, *Geophys. Res. Lett.,* **22,** 1045–1048.

Cevolini, G., 1994. The explosion of the bolide over Lugo di Romagna (Italy) on 19 January 1993, *Planet. Space. Sci.,* **42,** 767–775.

Dziewonski, A. & Anderson, D.L., 1981. Preliminary reference Earth model, *Phys. Earth planet. Inter.,* **25,** 297–356.

Georges, T.M., 1973. Infrasound from convective storms: examining the evidence, *Rev. Geophys. Space Phys.,* **11,** 571–594.

Hammel, H.R. *et al.,* 1995. HST imaging of atmospheric phenomena created by the impact of comet Shoemaker–Levy 9, *Science,* **267,** 1288–1296.

Ingersoll, A.P. & Kanamori, H., 1995. Waves from the collision of comet Shoemaker–Levy 9 with Jupiter, *Nature,* **374,** 706–708

Ingersoll, A.P., Kanamori, H. & Dowling, T.E., 1994. Atmospheric gravity waves from the impact of comet Shoemaker–Levy 9 with Jupiter, *Geophys. Res. Lett.,* **21,** 1083–1086.

Kanamori, H., 1993. Excitation of Jovian normal modes by an impact source, *Geophys. Res. Lett.,* **20,** 2921–2924.

Kanamori, H. & Mori, J., 1992. Harmonic excitation of mantle Rayleigh waves by the 1991 eruption of mount Pinatubo, Philippines, *Geophys. Res. Lett.,* **19,** 721–724.

Kanamori, H., Mori, J. & Harkrider, D.G., 1994. Excitation of atmospheric oscillations by volcanic eruptions, *J. geophys. Res.,* **22,** 21 947–21 961

Lavely, E.M. & Ritzwoller, M., 1992. The effect of global-scale, steady-state convection and elastic-gravitational asphericities on helioseismic oscillations, *Phil. Trans. R. Soc. Lond.* A, **339,** 431–496.

Liu, H.P, Anderson, D.L. & Kanamori, H., 1976. Velocity dispersion due to anelasticity; implications for seismology and mantle composition, *Geophys. J. R. astr. Soc.,* **47,** 41–58.

Lognonné, P., 1989. Modélisation des modes propres de vibration dans une Terre anélastique et hétérogène: théorie et application, *Thèse de Doctorat,* Unviersité de Paris VII, France.

Lognonné, P., 1991. Normal modes and seismograms in an anelastic rotating Earth, *J. geophys. Res.,* **96,** 20 309–20 319.

Lognonné, P. & Romanowicz, B., 1990. Fully coupled Earth's vibrations: the spectral method, *Geophys. J. Int.,* **102,** 365–395.

Lognonné, P., Mosser, B. & Dahlen, F.A., 1994. Excitation of the Jovian seismic waves by the Shoemaker–Levy 9 cometary impact, *Icarus,* **110,** 186–195.

Mosser, B. *et al.,* 1996. Impact seismology: a search primary pressure waves following impacts A and H, *Icarus,* **121,** 331–340.

Park, J. & Gilbert, F., 1986. Coupled free oscillations of an aspherical dissipative rotating Earth: Galerkin theory, *J. geophys. Res.,* **91,** 7241–7260.

Parrot, M. *et al.,* 1993. High frequency seismo-electromagnetic effects, *Phys. Earth planet. Inter.,* **77,** 65–83.

Pohhotelov, O.A., Parrot, M., Fedorov, E.N., Pilipenko, V.A., Surkov, V.V. & Gladychev, V.A., 1998. Response of the ionosphere to natural and man made acoustic sources, *Ann. Geophys.,* submitted.

Smith B.T., Boyle, J.M., Dongarra, J.J., Garbow, B.S., Ikebe, Y., Klema, V.C. & Moler, C.B., 1976. *Matrix Eigensystem Routines–EISPACK Guide,* Vol. 6, 2nd edn, *Lecture Notes in Computer Science,* Springer-Verlag, Berlin.

Suda, N., Nawa, K. & Fukao, Y., 1998. Incessant excitation of the Earth's free oscillations, *Science,* **279,** 2089–2091.

Takeuchi, H. & Saïto, H., 1972. Seismic surface waves, in *Methods in Computational Physics,* Vol. 11, pp. 217–295, ed. Bolt, B.A., Academic Press, New York.

Tanimoto, T., 1998. Excitation of normal modes by atmospheric turbulences: source of long period seismic noise, *Geophys. J. Int.,* submitted.

Tanimoto, T., Um, J., Nishida, K. & Kabayashi, N., 1998. Earth's continuous oscillations observed on seismically quiet days, *Geophys. Res. Lett.,* **25,** 1553–1556.

Tromp, J. & Dahlen, F.A., 1990. Free oscillations of a spherical anelastic earth, *Geophys. J. Int.,* **103,** 707–723.

Unno, W., Osaki, Y., Ando, H., Saio, H. & Shibahashi, H., 1989. *Non Radial Oscillations of Stars,* Tokyo University Press.

US Standard atmosphere, 1976. *Committee on the Extension to the Standard Atmosphere,* US Govt Printing Office, Washington, DC.

Watada, S., 1995. Part I: near-source acoustic coupling between the atmosphere and the solid Earth during volcanic eruptions, *PhD Thesis,* California Institute of Technology, Pasadena.

Weaver, P.F., Yuen, P.C., Prolss, G.W. & Furumoto, A.S., 1970. Acoustic coupling in the ionosphere from seismic waves of the earthquake at Kurile Islands on August 11, 1969, *Nature,* **226,** 1239–1241.

Widmer, R., & Zürn, W., 1992. Bichromatic excitation of long-period Rayleigh and air waves by the mount Pinatubo and El Chichón volcanic eruptions, *Geophys. Res. Lett.,* **19,** 765–768.

Woodhouse, J.H., 1988. The calculation of the eigenfrequencies and eigenfunctions of the free oscillations of the Earth and the Sun, in *Seismological Algorithms,* pp. 321–370, ed. Doornbos, D.J., Academic Press.

Woodhouse, J.H. & Dahlen, F.A., 1978. The effect of a general perturbation on the free oscillation of the Earth, *Geophys. J. R. astr. Soc.,* **53,** 335–354.

Yuen, P.C., Weaver, P.F., Suzuki, R.K. & Furumoto, A.S., 1969. Continuous traveling coupling between seismic waves and the ionosphere evident in May 1968 Japan earthquake data, *J. geophys. Res.,* **74,** 2256–2264.

Zürn, W. & Widmer, R., 1996. World wide observation of bichromatic long-period Rayleigh-waves excited during the June 15, 1991 Eruption of Mt. Pinatubo, in *Fire and Mud, Eruptions of Mount Pinatubo, Philippines,* pp. 615–624, eds Newhall, C. & Punongbayan, J.R., Philippine Institute of Volcanology and Seismology, Quezo City and University of Washington Press.

APPENDIX A: NON-DIMENSIONAL PROPAGATOR

We start from the form of Takeuchi & Saïto (1972):

$$\frac{d}{dr}\begin{pmatrix} Y_1 \\ Y_2 \\ Y_5 \\ Y_6 \end{pmatrix} = B \begin{pmatrix} Y_1 \\ Y_2 \\ Y_5 \\ Y_6 \end{pmatrix}, \tag{A1}$$

where

$$C=\begin{bmatrix} -\frac{2}{r}+\frac{\ell(\ell+1)g}{\omega^2 r^2} & \frac{1}{\kappa}-\frac{\ell(\ell+1)}{\omega^2\rho r^2} & \frac{\ell(\ell+1)}{\omega^2 r^2} & 0 \\ -\omega^2\rho-\frac{\ell(\ell+1)\rho g^2}{\omega^2 r^2}-4\frac{\rho g}{r} & -\frac{\ell(\ell+1)g}{\omega^2 r^2} & \frac{\rho g\ell(\ell+1)}{\omega^2 r^2}-(\ell+1)\frac{\rho}{r} & \rho \\ -4\pi\mathscr{G} & 0 & -\frac{\ell+1}{r} & 1 \\ 4\pi\mathscr{G}\left(-\frac{(\ell+1)}{r}\rho+\frac{\ell(\ell+1)g\rho}{\omega^2 r^2}\right) & -4\pi\mathscr{G}\frac{\ell(\ell+1)g}{\omega^2 r^2} & \frac{4\pi\mathscr{G}\rho\ell(\ell+1)}{\omega^2 r^2} & \frac{\ell+1}{r} \end{bmatrix}. \tag{A2}$$

We renormalize with the new variables

$$\begin{aligned} \tilde{Y}_1 &= r\sqrt{\rho g}\,Y_1, \\ \tilde{Y}_2 &= \frac{r}{\sqrt{\rho g}}\,Y_2, \\ \tilde{Y}_5 &= \frac{\sqrt{\rho g}}{4\pi\mathscr{G}}\,Y_5, \\ \tilde{Y}_6 &= \frac{\sqrt{\rho g}}{4\pi\mathscr{G}}\,Y_6, \end{aligned} \tag{A3}$$

to obtain the following:

$$\begin{pmatrix} r\sqrt{\rho g}r\frac{d}{dr}Y_1 \\ \frac{r}{\sqrt{\rho g}}r\frac{d}{dr}Y_2 \\ \frac{\sqrt{\rho g}}{4\pi\mathscr{G}}r\frac{d}{dr}Y_5 \\ \frac{\sqrt{\rho g}}{4\pi\mathscr{G}}r\frac{d}{dr}Y_6 \end{pmatrix} \frac{d}{dr}\begin{pmatrix} \tilde{Y}_1 \\ \tilde{Y}_2 \\ \tilde{Y}_5 \\ \tilde{Y}_6 \end{pmatrix} + \begin{pmatrix} \left(\frac{K}{2}-1\right)\tilde{Y}_1 \\ \left(-\frac{K}{2}-1\right)\tilde{Y}_2 \\ \frac{K}{2}\tilde{Y}_5 \\ \frac{K}{2}\tilde{Y}_6 \end{pmatrix}. \tag{A4}$$

Substituting eq. (A1) into eq. (A4), we finally obtain the main expression in the text, eq. (21).

APPENDIX B: CUT-OFF FREQUENCIES

We consider the characteristic equation (25). The roots λ are given by

$$\begin{aligned} \lambda^2 &= C_{11}^2 + C_{21}C_{12} \\ &= \left(1+\frac{K}{2}-\frac{\ell(\ell+1)}{\tilde{\omega}^2}\right)^2 - \left(4+\tilde{\omega}^2-\frac{\ell(\ell+1)}{\tilde{\omega}^2}\right)\left(V_g-\frac{\ell(\ell+1)}{\tilde{\omega}^2}\right), \end{aligned} \tag{B1}$$

where $V_g = gr/c^2$ and $\tilde{\omega}^2 = \omega^2 r/g$ is the non-dimensional angular frequency. Expression (B1) can be rewritten as

$$\lambda^2 = -\frac{1}{\tilde{\omega}^2}\left(V_g\tilde{\omega}^4+\tilde{\omega}^2\left(4V_g-\ell(\ell+1)-\left(1+\frac{K}{2}\right)^2\right)+\ell(\ell+1)\frac{N^2 r}{g}\right., \tag{B2}$$

where we have used the Brunt–Vaissala frequency, defined as

$$\frac{N^2 r}{g} = -\left(\frac{r}{g}\partial_r\rho+\frac{gr}{c^2}\right) = K-2-V_g. \tag{B3}$$

Eq. (B2) has two roots $\pm\Delta$ and can be rewritten as

$$\Delta^2 = -\frac{V_g}{\tilde{\omega}^2}(\tilde{\omega}^2-\tilde{\omega}_1^2)(\tilde{\omega}^2-\tilde{\omega}_2^2). \tag{B4}$$

A real value of Δ is found only for $\tilde{\omega}$ in the interval bounded by $\tilde{\omega}_1$ and $\tilde{\omega}_2$. For such a frequency, the modes are trapped. For angular frequencies smaller than $\tilde{\omega}_1$, the modes are gravity modes. For angular frequencies higher than $\tilde{\omega}_2$, the modes are acoustic modes (Fig. B1). In both cases, however, the modes are not trapped and the two roots define solutions with either upward or downward propagation.

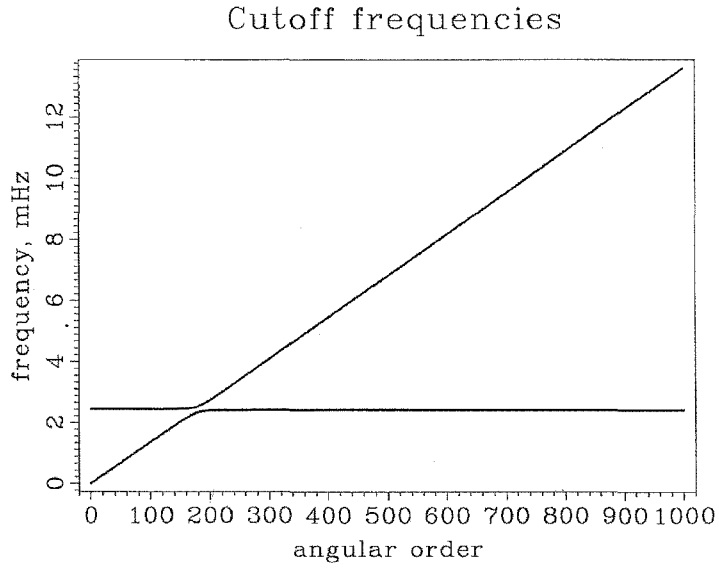

Figure B1. The two roots of eq. (B4) are shown with respect to the angular order ℓ and the frequency. The domains for the trapped modes and for the propagating modes are indicated. These roots are calculated for the atmospheric model at 150 km, where the boundary condition is applied.

APPENDIX C: DEFINING THE BASIS FUNCTIONS

We define the boundary condition operator $\mathscr{M}_0(\mathbf{u})$ as

$$\mathscr{M}_0^i(\mathbf{u}) = \mathbf{T}^{ij}_{\text{elastic}}(\mathbf{r}, t)\, n_j\,, \tag{C1}$$

where $\mathbf{T}_{\text{elastic}}$ is the stress associated with the displacement $\mathbf{u}$, and n_j is the radial normal vector. This operator associates each displacement field with the stress vector at the horizontal (spherical) interface. In the solid area, it is invertible (e.g. has a null kernel) with the exception of block rotation. In the fluid areas, it has only one non-zero component $[\mathscr{M}_0^r(\mathbf{u})]$, and has a non-null kernel associated with secular motions, which induce zero stress in the fluid parts (e.g. differential axisymmetric rotations). When this operator is applied to a solution of the free surface problem $\mathbf{u}$, the vector $\mathscr{M}_0(\mathbf{u})$ is continuous and vanishes at the free surface.

We now consider a continuous function $\mathbf{f}$ vanishing at the top of the model whose two horizontal components are null in the fluid parts. The displacement field $\boldsymbol{v}$, defined as

$$\boldsymbol{v} = \mathscr{M}_0^{-1}(\mathbf{f})\,, \tag{C2}$$

obtained using the integral inverse operator of the boundary condition, obviously satisfies the boundary conditions. Because the set of spherical normal modes define a complete set of functions, $\boldsymbol{v}$ can be written as follows:

$$\boldsymbol{v} = \sum_k c_k \mathbf{u}_k\,. \tag{C3}$$

Here the sum over k denotes all the eigenfunctions that do not belong to the kernel of $\mathscr{M}_0$. Using the operator $\mathscr{M}_0$, this relation becomes

$$\mathbf{f} = \sum_k c_k \mathscr{M}_0(\mathbf{u}_k)\,. \tag{C4}$$

More generally, we consider a displacement field $\boldsymbol{v}$ that satisfies the 'open' boundary conditions. It can be written in the following form:

$$\boldsymbol{v} = \mathscr{M}^{-1}(\mathscr{M}(\boldsymbol{v})) + \boldsymbol{v}'\,, \tag{C5}$$

where $\boldsymbol{v}'$ is the projection of $\boldsymbol{v}$ on the kernel of operator $\mathscr{M}$. Using relation (C4), we then have

$$\boldsymbol{v} = \sum_k c_k \mathscr{M}^{-1}(\mathscr{M}_0(\mathbf{u}_k)) + \boldsymbol{v}'\,. \tag{C6}$$